Check for updates

Metal–organic framework (MOF) facilitated highly stretchable and fatigue-resistant ionogels for recyclable sensors†

Qunmeng Xia, [ID] ‡ Weizheng Li,‡ Xiuyang Zou, [ID] Sijie Zheng, Ziyang Liu, [ID] Lingling Li and Feng Yan [ID] *

Ionogel-based flexible sensors are widely applied in wearable biomedical devices and soft robots. However, the abandoned ionic sensors are rapidly turning into e-waste. Here, we harness the porosity and the coordination of metal sites of metal–organic frameworks (MOFs) to develop physically crosslinked ionogels, which are composed of polymer chains that coordinate with the MOF metal sites. The covalent crosslinking of the host material transformed into reversible bond interactions that significantly enhance the mechanical properties of the MOF-ionogels. The obtained ionogels can endure an 11 000% stretch and exhibit Young's modulus and toughness of 58 MPa and 25 MJ m^{-3}, respectively. In addition, the fracture energy is as high as 125 kJ m^{-2}, outperforming most reported ionogels. Furthermore, the UiO-66-ionogels are fully recyclable and both the mechanical and electrical properties can be restored. The results of this work provide a new vision for the development of future "green" sensors.

New concepts

Ionogel-based flexible sensors are widely applied in wearable biomedical devices and soft robots. However, chemically crosslinked ionogels incur irreversible damage after prolonged use and rapidly turn into e-waste. To this end, physically crosslinked ionogels have been developed for long-term use and recycling. Here, we harness the porosity and the coordination of metal sites of metal–organic frameworks (MOFs) to develop physically crosslinked ionogels, which are composed of polymer chains that coordinate with the MOF metal sites. The coordination between the MOFs and the polymer segments prevents covalent cross-linking in the matrix polymer network, endowing the ionogels with sufficient energy dissipation, high mechanical properties, and recyclability for applications in flexible electronic devices. We expect that our work can provide a new vision for the development of future "green" electronic devices.

Introduction

Ionogels (or ionic conductors), which are composed of ionic liquids (ILs), have attracted significant attention in recent years because of their nonvolatility, high thermal stability, ionic conductivity, and incombustibility.[1–8] Owing to their special properties, ionogels can be used in various applications, such as solid electrolytes,[9] strain sensors,[10,11] soft robotics,[12] and ionic skins.[13–15] To further extend the applicability of ionogels, different strategies that combine the various desirable properties of ionogels including high mechanical strength and elasticity,[16–19] self-healing ability,[20] recyclability, and self-adhesiveness have

been adopted.[21] Significant efforts have been devoted over the past decade to developing ionogels with high mechanical strength, which is necessary for practical applications. In developing high-strength and tough hydrogels, great progress has been made over the past decade, which can be used to toughen ionogels in principle. The addition of metal ions has been found to increase the crosslink density of ionogels and thus toughen them.[22–25] Ionogels are also strengthened by the presence of dynamic and strong sacrificial metal coordination bonds. Furthermore, the addition of nanoparticles to the ionogel polymer network introduces sufficient energy dissipative units that effectively toughen the gel. However, because of poor compatibility between the nanoparticles and polymer chains, additional chemical crosslinking agents must be introduced into the polymer networks, which renders them rigid and irreversible.[11,18,26–31]

During the past few years, novel ionogels with good properties have been prepared and successfully applied for stretchable ionic skins and sensors;[10,11,13–15] however, the increasing amount of e-waste has raised more and more attention.[32–39] In this study, we synthesized a class of physically crosslinked multifunctional ionogels, through the coordination of polymer

Jiangsu Engineering Laboratory of Novel Functional Polymeric Materials, Jiangsu Key Laboratory of Advanced Negative Carbon Technologies College of Chemistry, Chemical Engineering and Materials Science, Soochow University, Suzhou, 215123, China. E-mail: fyan@suda.edu.cn

† Electronic supplementary information (ESI) available. See DOI: **https://doi.org/10.1039/d2mh00880g**

‡ Authors with equal contributions.

chains and MOFs, which increased the crosslink density. MOFs, which are highly crystalline materials, composed of metal nodes and organic ligands, have attracted significant attention because of their porosity, high surface areas, and physiochemical properties.[40–42] The proposed polymer network topology is novel and reversible, which can endow ionogels with excellent mechanical properties and recyclability. Furthermore, MOF addition reduced notch sensitivity, prevented crack propagation at the crack tip, and significantly enhanced the fatigue resistance of the ionogels, therefore showing promising applications in flexible and recyclable electronic devices.

Results and discussion

Preparation and characterization of UiO-66-ionogels

Scheme 1 shows a schematic of ionogel preparation using UiO-66 (Zr-MOF) as points. A mixture was prepared by dispersing N,N-dimethylacrylamide (DMAA), 1-cyanomethyl-3-methylimidazolium bis[(trifluoromethyl)sulfonyl]imide ([CMMIM][TFSI]), UiO-66 (pore size: ~ 2.8 nm, Fig. S3, ESI†), and 1-hydroxycyclohexyl phenyl ketone (HCPK, photoinitiator). The mixture was then stirred for 3 h to obtain a homogeneous precursor solution. The monomer, DMAA, can enter the pores of UiO-66 due to its relatively smaller size. Then, the mixture aggregated upon exposure to 365 nm UV light. The polymer chains were linked with UiO-66 through reversible bonds such as coordination, which endowed the UiO-66-ionogel with excellent mechanical properties.

The reversible interactions inside the UiO-66-ionogels that endow them with excellent mechanical properties were characterized. The ^{1}H NMR spectra indicated that with the addition of DMAA, the imidazole peaks corresponding to active hydrogen ions (positions 2, 4, and 5) shifted to lower fields, indicating the formation of hydrogen bonds between IL and DMAA (Fig. 1a). Fig. 1b shows the Fourier transform infrared (FT-IR) spectroscopy of DMAA, IL, and DMAA/IL. A C=O vibrational peak of DMAA initially appeared at 1647 cm^{-1} and then shifted to 1635 cm^{-1}, and a C–N vibrational peak of the imidazolium cation ring initially appeared at 1619 cm^{-1} and then shifted to 1598 cm^{-1}.[43] These significant shifts to lower wavenumbers indicated strong intermolecular interactions between the IL and DMAA. Fig. S4 (ESI†) also illustrates the presence of hydrogen bonds. The peak intensity related to hydrogen bonded –C=O at 1628 cm^{-1} decreases from 30 to 140 °C, while the peak intensity at 1742 cm^{-1} of free –C=O is increased. Furthermore, UiO-66-ionogel with an IL content of 90 wt% was characterized in different frequency ranges via rheological measurements. The storage modulus (G') of the ionogel at different frequencies was greater than the loss modulus (G''), but both G' and G'' were stable (Fig. S5, ESI†). Intermolecular interaction enhanced the stability of the ionogel and enabled it to prevent leakage. Thermogravimetric analysis (TGA) was used to investigate the thermal stability of the UiO-66-ionogel. As shown in Fig. S6 (ESI†), the UiO-66-ionogel exhibited thermal stability in temperatures up to 250 °C in a nitrogen atmosphere and long-term thermal stability in
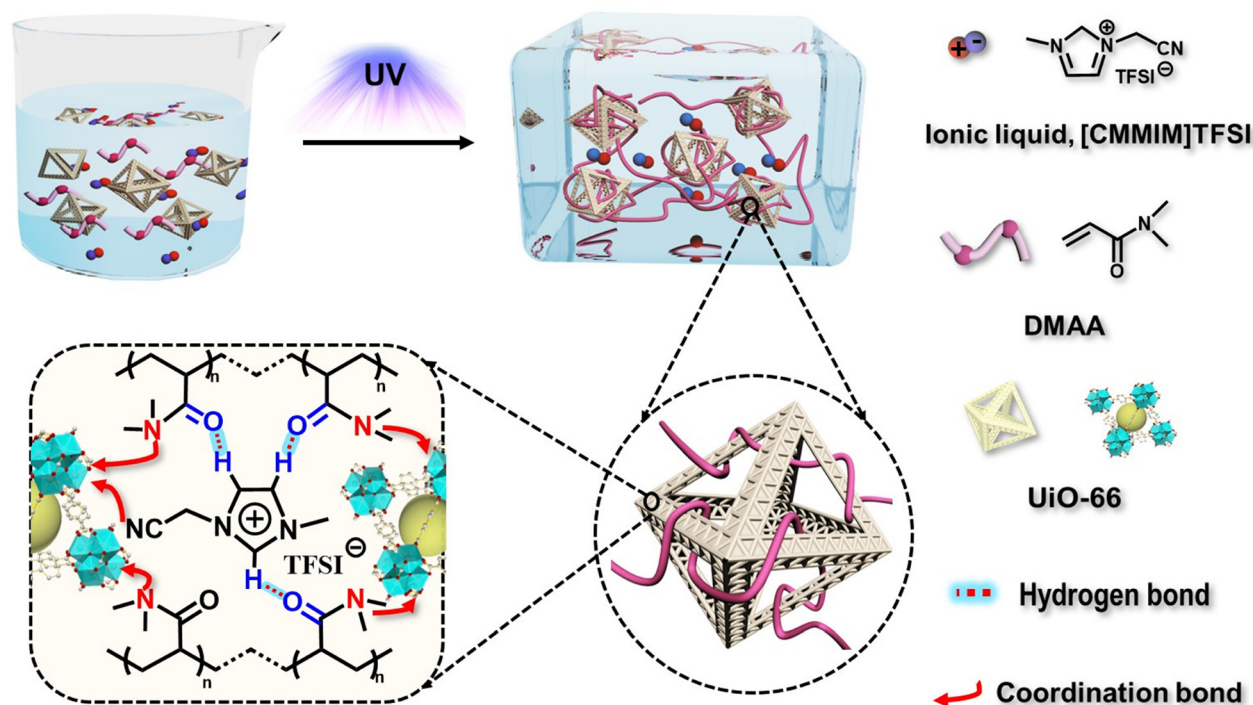
Scheme 1 Schematic of the preparation of UiO-66-ionogels. UiO-66 was mixed with N,N-dimethylacrylamide (DMAA), and 1-cyanomethyl-3-methylimidazolium bis[(trifluoromethyl)sulfonyl]imide ([CMMIM]TFSI), which resulted in the formation of a linear network with interpenetrating entangled topology after polymerization of the monomers. The polymer chains and [CMMIM]TFSI interacted with the metal sites of UiO-66 and thus formed physically crosslinked UiO-66-ionogels.
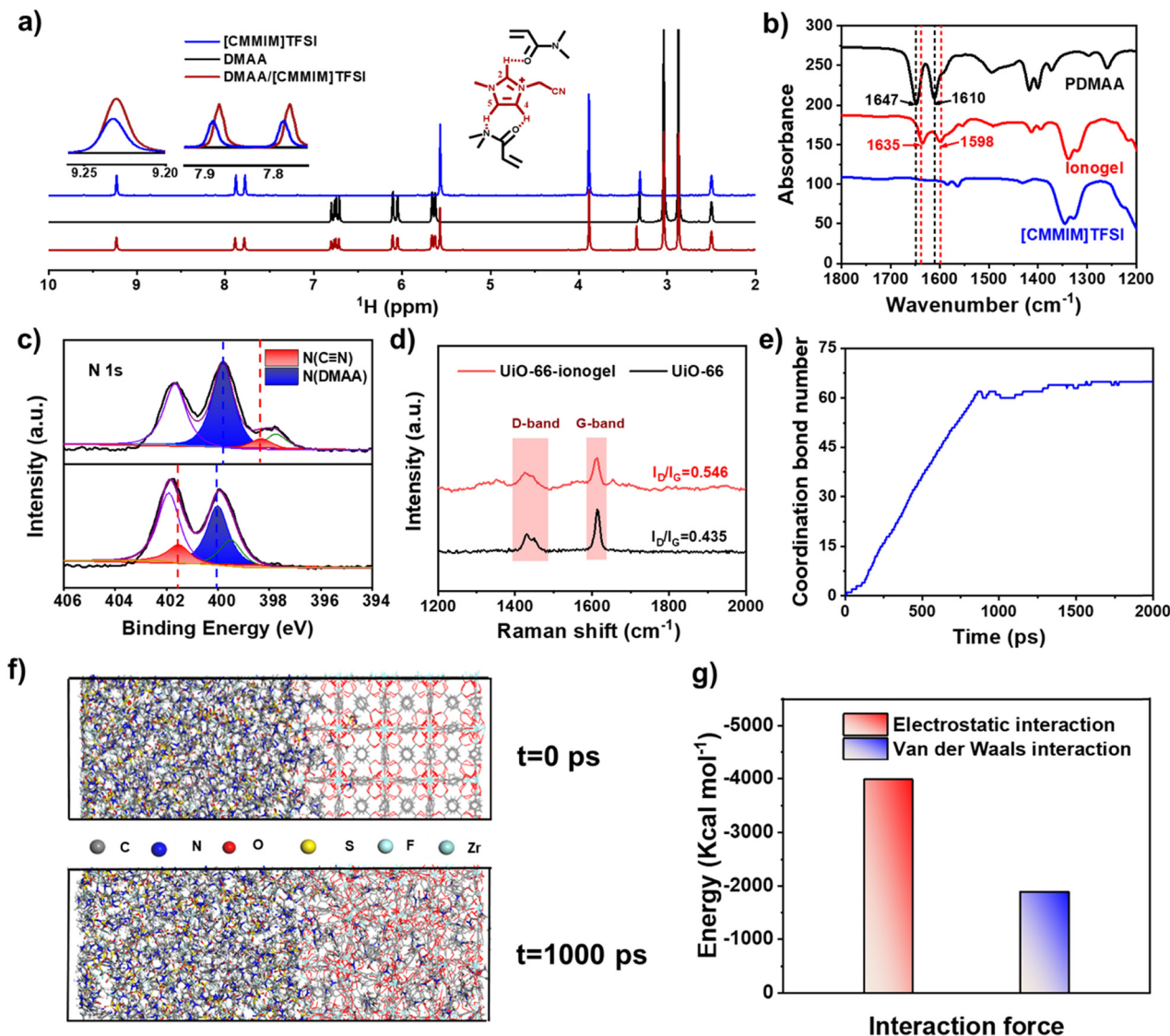
Fig. 1 Characterization of the reversible dynamic bonds in the UiO-66-ionogel. (a) ^{1}H NMR spectra of DMAA, [CMMIM]TFSI, and DMAA/[CMMIM]TFSI. The insets show hydrogen bonds between [CMMIM]TFSI and DMAA. (b) FT-IR spectra of PDMAA, [CMMIM]TFSI, and UiO-66-ionogel. (c) N 1s XPS results for the pure polymer and UiO-66/polymer. (d) Raman spectra of UiO-66 and UiO-66-ionogel. (e) Coordination bond number between UiO-66 and IL. (f) Snapshot of the MD system showing DMAA in UiO-66. (g) The energy of electrostatic and van der Waals interactions between DMAA and UiO-66 using MD simulations.

temperatures up to 200 °C in air and nitrogen. The weight of the UiO-66-ionogel remained unchanged for a long time, indicating that it possesses excellent thermal stability. As shown in Fig. 1c and Fig. S7 (ESI†), the coordination between the cyano group of the IL, the amide groups of the pure polymer and the Zr ion of UiO-66 was characterized by X-ray photoelectron spectroscopy (XPS). The N 1s core-level spectrum of pure polymer was fitted using four well-resolved components at 401.6, 399.7, 398.5, and 397.7 eV, which were attributed to the N atoms of the imidazolium cation ring, the N–C bonds of DMAA, the cyano groups of [CMVIM]Br, and the H–N–C bonds of MBAA, respectively. As for the UiO-66/polymer, the N 1s core-level spectrum was fitted using four well-resolved components at 401.9, 401.6, 400, and 399.5 eV, which were attributed to the N atoms of the imidazolium cation ring, cyano groups of

[CMVIM]TFSI, N–C bonds of DMAA, and H–N–C bonds of MBAA, respectively. Compared with N atoms (399.7 eV) in the amide groups of the pure polymer, the corresponding peak in the UiO-66-polymer was shifted to 401.6 eV indicating that a charge transfer occurred between the amide group and UiO-66/polymer, because of the coordination effect of Zr in UiO-66.[44] Raman spectroscopy was also used to analyze the interaction between the polymer and UiO-66 (Fig. 1d); the Raman spectra of both UiO-66 and the UiO-66-ionogel indicate the presence of the D band (1425 cm^{-1}) and G band (1610 cm^{-1}).

The value of I_D/I_G (intensity ratio of D band and G band) was 0.435 for UiO-66 and 0.546 for the UiO-66-ionogel, indicating that the symmetry of the UiO-66 structure decreased, which was caused by the strong interaction between the polymer and UiO-66.[45,46] The interaction between the DMAA and IL with UiO-66

was investigated by molecular dynamics (MD) simulations. Coordination bonds could be observed between IL and UiO-66, as illustrated in Fig. 1e. Fig. 1f shows the initial and the most stable states of the solvent and UiO-66 molecular model system with minimum energy after optimization and equilibration. It can be seen that the DMAA molecules enter the pores of UiO-66 due to the electrostatic and van der Waals forces (Fig. 1g).

Mechanical properties

To optimize the mechanical properties, a series of UiO-66-ionogels were synthesized with different IL contents (50–90 wt%) and UiO-66 (0.1–2 wt%). As shown in Fig. 2a, the obtained ionogels exhibited excellent mechanical strength and stretchability. In particular, when the content of the IL was increased, the elongation at break of the ionogels improved. When the IL content was increased from 50 wt% to 90 wt%, the fracture strength of the UiO-66-ionogels decreased from 7.6 MPa to 225 kPa, while the strain at fracture increased from 15% to 11 000%, because the density of the polymer network was affected by the content of IL. Therefore, with increasing cross-link density, the strain decreased. The higher polymer content makes UiO-66-ionogel less deformable and brittle. For example, when the IL content was 50 wt%, the maximum Young's modulus of the UiO-66-ionogel was 58 MPa (Fig. 2b), while the fracture strain rapidly decreased to 15%. The UiO-66-ionogel also exhibited high maximum toughness of 25 MJ m^{-3} (Fig. 2b), which was attributable to the sliding and migration of UiO-66 nanoparticles during the tensile process. Moreover, the content

of UiO-66 influenced the crosslinking density of the ionogel (Fig. 2c and d). With increasing the content of UiO-66, the crosslinked network became tighter, and the macroscopic stress and strain increased and decreased, respectively. Furthermore, energy dissipation occurred mainly due to a large number of physical interactions (such as hydrogen and coordination bond interactions) and stress transfer effects. As the stress transfer center in the polymer network, UiO-66 effectively transferred the external stress to the surrounding polymer chain without allowing the stress concentration to break the network. Due to the coordination of the polymer chains with UiO-66, the overall mechanical properties of the ionogels improved significantly. The ionogel with an IL content of 90 wt% exhibited a tensile strain of 11 000%, which is considerably higher than the tensile properties of most existing ionogels (Fig. 2e).

The mechanical properties of the obtained ionogels were further analyzed. The UiO-66-ionogel exhibits insensitivity toward crack propagation after the introduction of a notch, as shown in Fig. 3a. Notably, the notched ionogel could be stretched up to 7600%, indicating that the ionogels possessed excellent tear resistance. As shown in Fig. 3b, the corresponding crack propagation strain and energy required to fracture the notched UiO-66-ionogels with different IL contents were quantified and calculated. By contrast, the ionogel without additives fractured easily (Fig. S8, ESI†), and the energy dissipation was inherent due to fracture in the polymer chain. Furthermore, rapid propagation of cracks occurred because the stress was rapidly concentrated at the crack or weak crosslinking points. However, when external force was applied to the notched
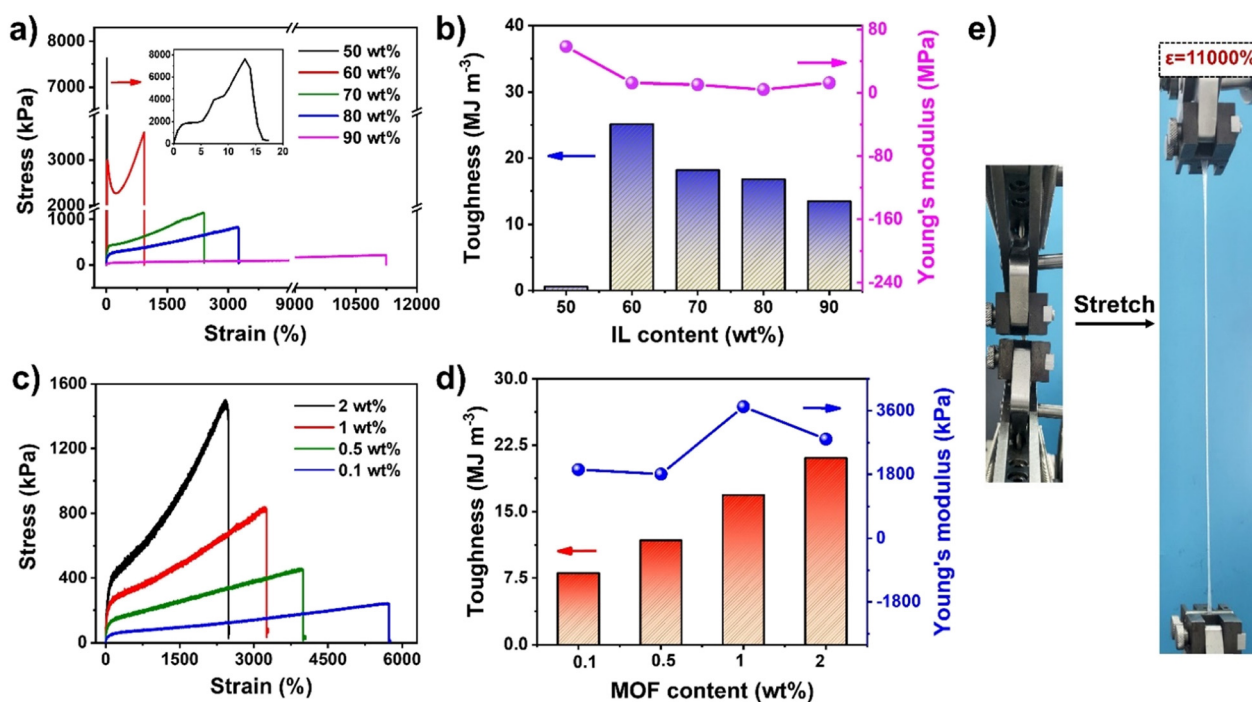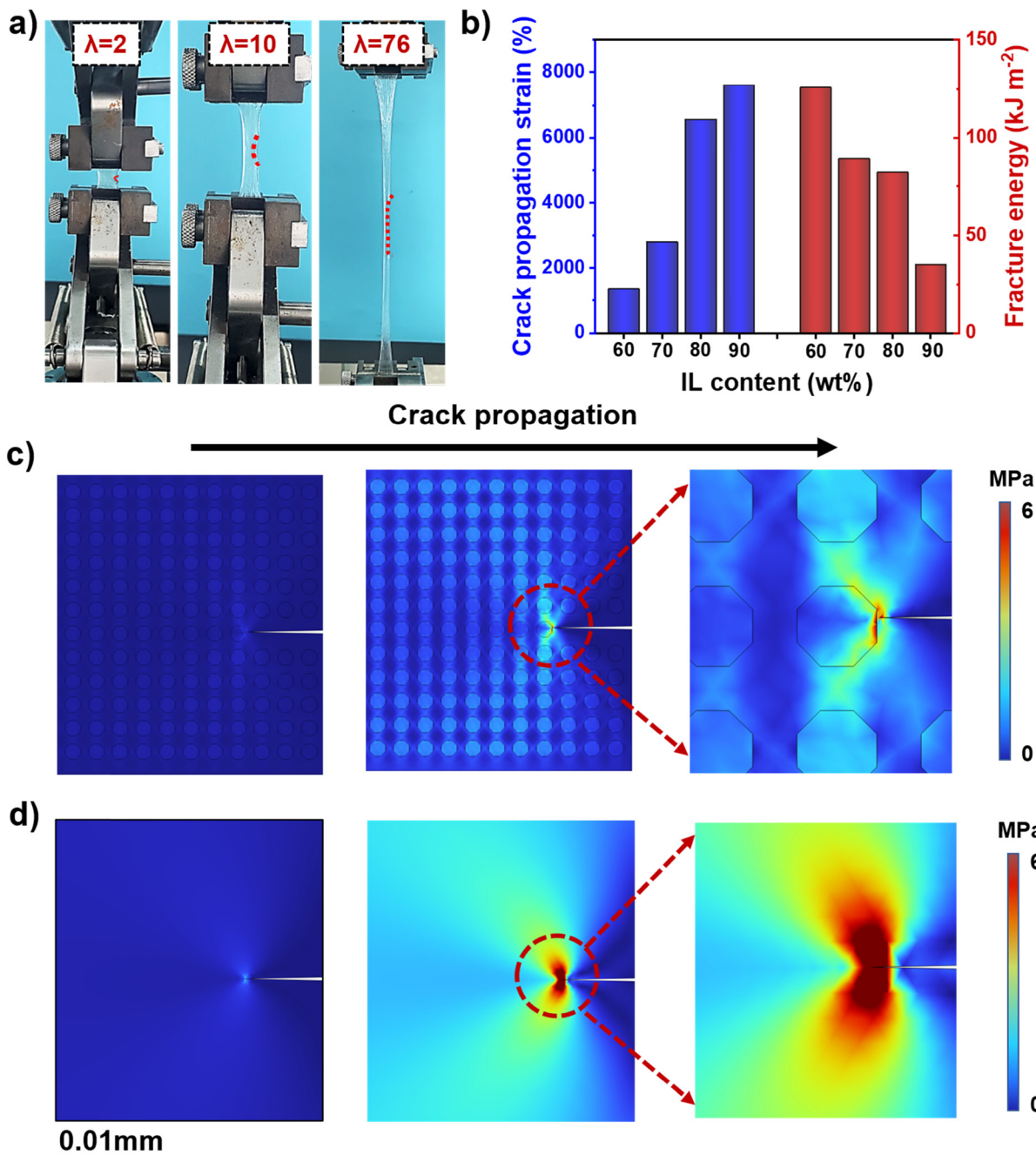

Fig. 2 Mechanical properties of UiO-66-ionogels. (a) Monotonic tensile stress–strain curves, (b) toughness, and Young's modulus of the UiO-66-ionogels with different IL contents and 1.0 wt% UiO-66. (c) Monotonic tensile stress–strain curves, (d) toughness, and Young's modulus of UiO-66-ionogels with different UiO-66 contents and 80 wt% IL. (e) Stretchability of the UiO-66-ionogel (IL: 90 wt%, UiO-66: 1.0 wt%) up to 11 000% of the original.

Fig. 3 Mechanical properties of UiO-66-ionogels. (a) Monotonic variations in tensile properties of a notched UiO-66-ionogel (linearly notched for 15% of the specimen width). (b) Corresponding crack propagation strains and calculated fracture energies of UiO-66-ionogels with different IL contents. The content of UiO-66 used in the notched samples was 1 wt%. Finite element simulations of the stress distribution inside the (c) UiO-66-ionogel and (d) ionogel containing 0.5 wt% chemical crosslinking agent (MBAA).

UiO-66-ionogel, UiO-66 transferred the stress to the polymer chains, which effectively passivated and eliminated crack tip propagation and increased the fracture energy.

As shown in Finite element simulations (Fig. 3c and d and Fig. S9, ESI†), UiO-66 can inhibit crack propagation effectively, illustrating the role of UiO-66 in dissipating fracture energy. Moreover, the UiO-66-ionogel could be inflated with nitrogen like a balloon and deformed reversibly in all directions, thereby indicating that the ionogel possessed high ductility and

excellent mechanical properties (Fig. 4a). The viscoelasticity of the ionogel was further analyzed *via* cyclic tensile tests. The elasticity of the ionogel was maintained even after 30 stretching cycles at 500% predetermined strain (Fig. 4b), indicating that the UiO-66-ionogel recovered well. Elasticity and cycling stability (*i.e.*, durability) of materials are necessary for flexible devices. After 20 000 compression cycles, the ionogel remained elastic, thereby indicating good fatigue resistance (Fig. 4c). The UiO-66-ionogel developed in this study exhibited superior
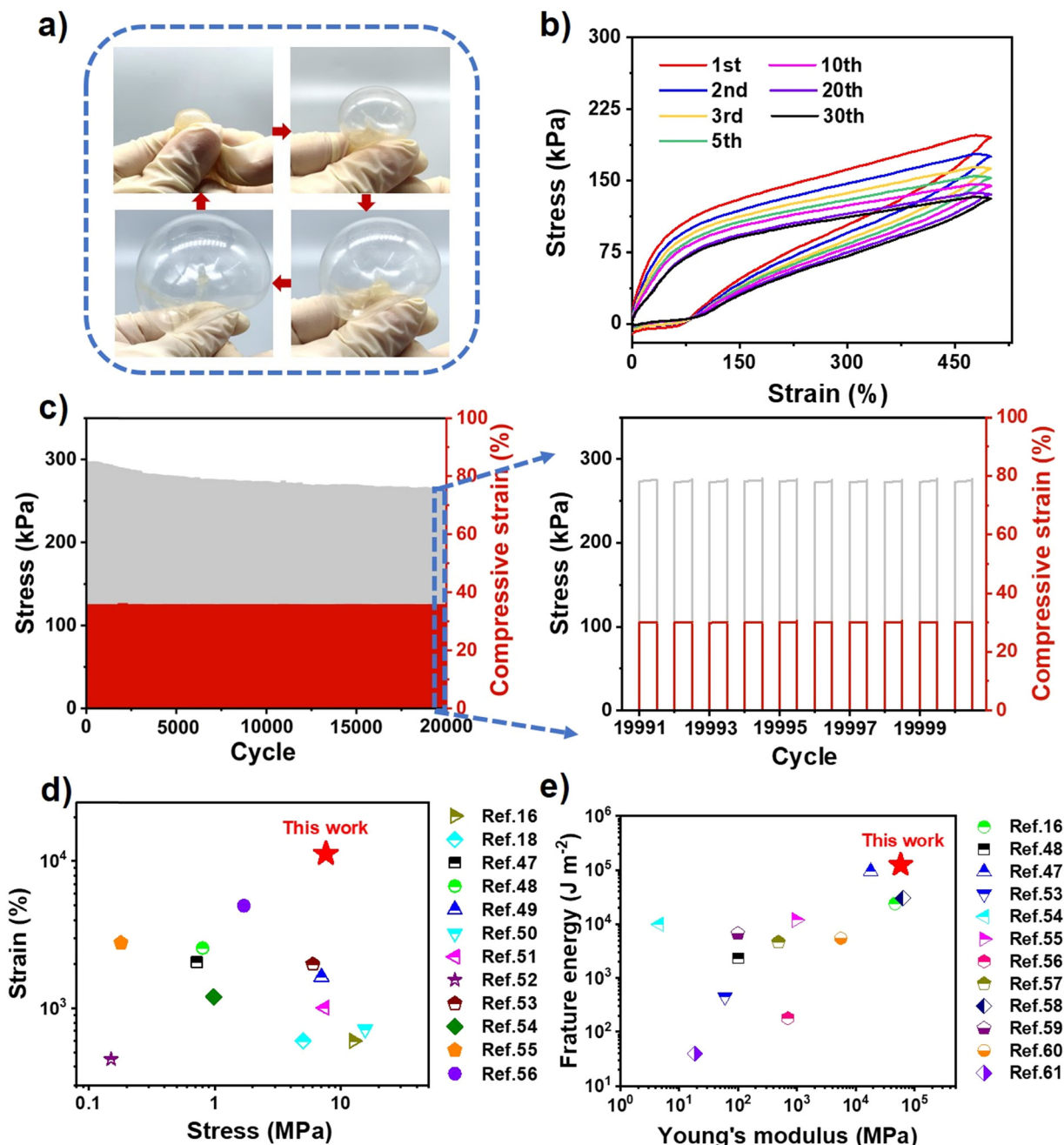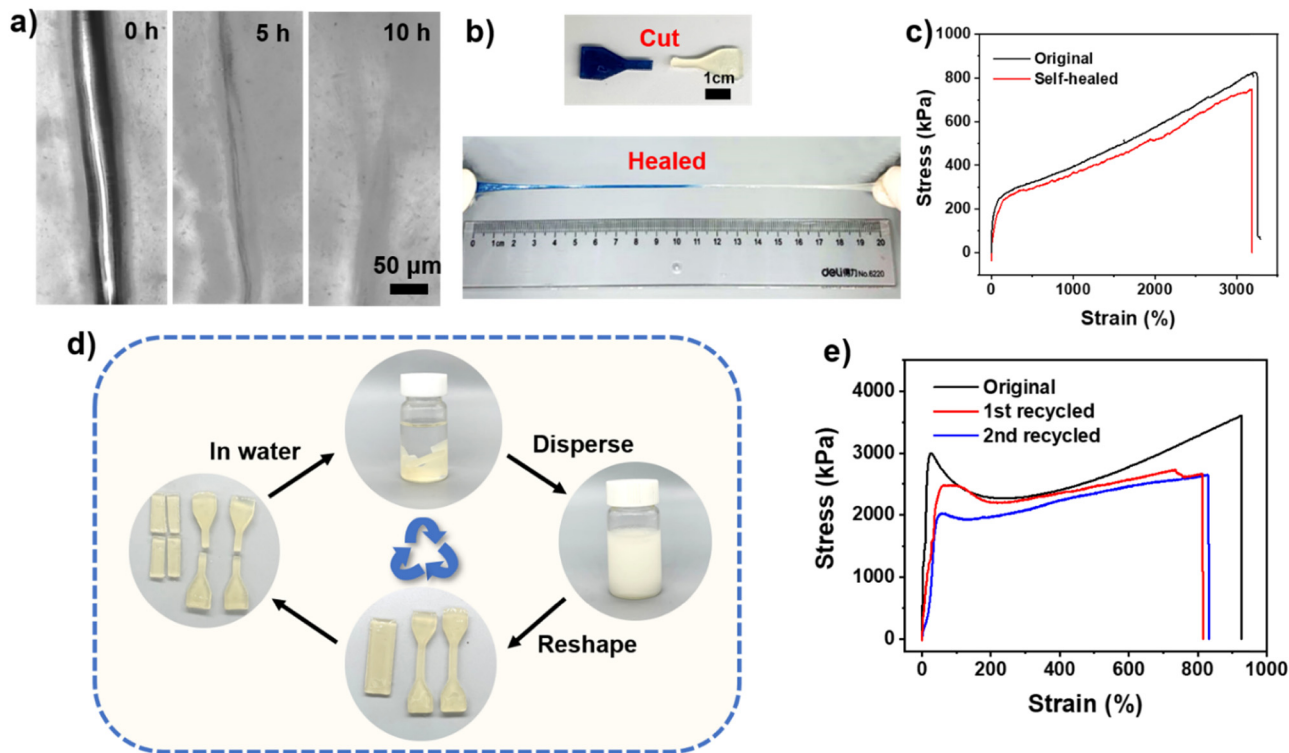
Fig. 4 Mechanical properties of UiO-66-ionogels. (a) UiO-66-ionogel (2×2 cm^2) could be inflated by nitrogen and demonstrated excellent toughness. (b) UiO-66-ionogel could be compressed over 20 000 cycles at 30% strain (with 30 s intervals). (c) Cyclic stress–strain curves of the UiO-66-ionogel at 500% with 1 min intervals. (d and e) Comparison of the mechanical properties (strain, stress, Young's modulus, and fracture energy) between UiO-66-ionogels and recently reported ionogels.

mechanical properties compared with representative gels in recent literature, as shown in Fig. 4d[16,18,47–56] and Fig. 4e.[16,48,53–61] The fracture energy (125 kJ m^{-2}) and Young's modulus (58 MPa) of the UiO-66-ionogels (Fig. 2b and 3b) are considerably higher than those of existing gels (Fig. 4e).

Self-healing and recyclable properties

The self-healing and recyclable properties of materials can measurably extend the service life of materials and equipment.

Multiple reversible interactions (such as coordination bonds, hydrogen bonds, and electrostatic interaction) endowed the UiO-66-ionogel with excellent self-healing ability. The self-healing process of the ionogel at room temperature was analyzed by monitoring the damaged interface using an optical microscope at different times. After approximately 10 h at room temperature, the crack in the ionogel nearly disappeared (Fig. 5a). As shown in Fig. 5b, two dumbbell-shaped samples of different colors (one was dyed blue) were sliced in half and

Fig. 5 Self-healing and recyclable properties of UiO-66-ionogels. (a) Images of completely severed specimens were obtained using an optical microscope at different self-healing times at 25 °C. (b) The pieces of the self-healing ionogel merged together; the ionogel was healed and could be stretched. (c) Monotonic variations in the tensile stress–strain curves of UiO-66-ionogel after self-healing. After self-healing at 25 °C for 10 h, the mechanical properties (stress and strain) of the UiO-66-ionogel could nearly be restored to their original state. (d) Schematic of the recyclability of the UiO-66-ionogels. (e) Tensile stress–strain curves of the UiO-66-ionogel after reconstruction and the mechanical properties could be recovered.

allowed to heal at room temperature. After approximately 10 min, two slices were tightly stuck together (Fig. S10, ESI†). The healing efficiency of the ionogel was evaluated through tensile stress–strain tests. The healing efficiency of the ionogel was approximately 99% after 12 h of self-healing at room temperature (Fig. 5c). UiO-66-ionogel can be reversibly bent or twisted without fracture, and it can self-heal even under −20 °C (Fig. S10, ESI†). The glass transition temperatures of the IL and DMAA were −38 °C and −37 °C, respectively. After polymerization, the glass transition temperature of the UiO-66-ionogel decreased to −42 °C (Fig. S11, ESI†). The rapid recovery could be attributed to the existence of multiple reversible interactions (such as hydrogen bond, coordination bonds, and electrostatic interaction) at the fracture interface of the UiO-66-ionogel. Ionogels are often used for the fabrication of stretch sensors. However, the ionogels undergo irreversible failure after long-term use predominantly because the rigid irreversible covalent bonds are damaged, after which the ionogel cannot be recovered or regenerated. The UiO-66-ionogels obtained in this study were recyclable and applicable to different situations due to the non-covalent bonds (coordination bonds, electrostatic interaction, and hydrogen bonds). As shown in Fig. 5d, the UiO-66-ionogels were dispersed in deionized water to obtain a homogeneous dispersion, which was then poured into molds of different shapes. We speculate that due to the limitation of the pores of UiO-66, the polymer chains inside

UiO-66 cannot come out, and this part exists in the form of ionogel fragments. Meanwhile, other parts are reversibly untangled because of the stronger hydrogen bonds with water molecules. After the water evaporated, UiO-66-ionogels of different shapes were obtained. The recovered UiO-66-ionogels demonstrated excellent mechanical properties and excellent remolding properties of UiO-66-ionogels (Fig. 5e). Therefore, the ionogels can be regenerated by rearranging and disentangling the MOF and polymer chains and reorganizing the hydrogen bonds.

Electrical sensing properties of UiO-66-ionogel

The IL endowed UiO-66-ionogel with high electrical conductivity because of ion migration in the ionogels. In Fig. 6a, both ends of the UiO-66-ionogel were connected to the conductive copper foil, and a simple resistivity sensor was obtained. The temperature was controlled using a heating table and a refrigerator, and the resistance changes of the UiO-66-ionogel were monitored to analyze its temperature sensing properties. As shown in Fig. 6b, the resistance of the ionogel decreased with an increase in temperature. Furthermore, the periodic stretching and relaxation of the sensor corresponded to accurate and reversible resistance responses (Fig. 6c). Fig. 6d shows the changes in relative resistance of the UiO-66-ionogel under the combined influence of temperature variations and stretching. The decrease in temperature and stretching increased the relative resistance of the ionogel.
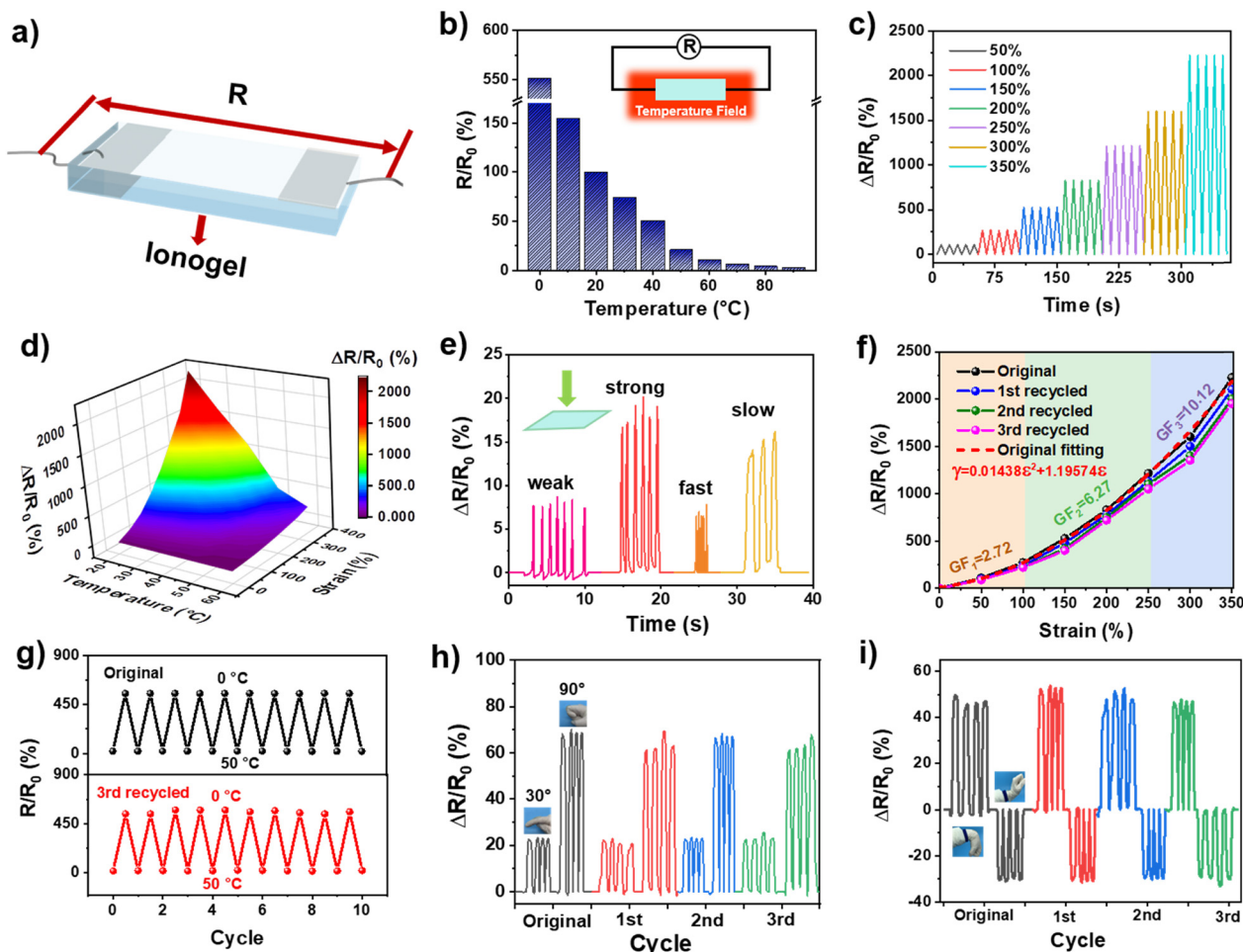
Fig. 6 Electrical sensing properties of the original ionogel. (a) Schematic of the flexible intronic sensor fabricated using the UiO-66-ionogel. (b) Changes in the resistance of the UiO-66-ionogel with variations in temperature. (c) Real-time monitoring of the relative resistance under different strains between 50% and 350%. (d) Influence of temperature and strain on the resistive signals of the UiO-66-ionogel. (e) Signals of relative electrical resistance during pressing. (f) Changes in the relative resistance of the original and recycled UiO-66-ionogel with variations in tensile strain. (g) Dynamic responses of the original and recycled UiO-66-ionogel over 10 cycles when the ionogel was subjected to heating and cooling between 0 °C and 50 °C. After the recycling of the sensor, its resistance response to temperature is basically unchanged. The original and recycled UiO-66-ionogel can be used to monitor the movement of (h) finger bending, and (i) wrist bending, and the electrical properties can be recovered after recycling.

We also detected the electrical resistance signal of the UiO-66-ionogel for pressing, and the results showed that the UiO-66-ionogel has good responsiveness (Fig. 6e). The relative resistance ($\Delta R/R_0$) of the resistivity sensor was monitored within the different strain ranges from 0 to 350% (Fig. 6f). The parabolic equation ($\gamma = 0.01438\varepsilon^2 + 1.19574\varepsilon$) with a high correlation coefficient ($r^2 = 0.998$) was fitted according to the relative resistance data at different strains; ε denoted tensile strain. To evaluate the sensitivity of the sensor, the gauge coefficient (GF) and the change in relative resistance under the applied strain were calculated from the fitting curve. The ionogel possessed high sensitivity within the measured strain ranges; the GF was 2.72, 6.72, and 10.12 under 100%, 100–250%, and 250–350% strain, respectively. To further prove that the recycled UiO-66-ionogel still has good electrical resistance responsiveness, the tensile electrical resistance responsivity was tested. The results demonstrated that the difference in tensile resistance responsivity between the recycled UiO-66-ionogel

sensor and the original sensor is negligible. The temperature cycling stability of the device was further analysed by subjecting it to continuous heating and cooling between 0 °C and 50 °C. The resistance responses of the original and recycled ionogel were nearly constant over 20 cycles, thereby indicating excellent cycling stability (Fig. 6g). As shown in Fig. 6h and Fig. S13 (ESI†), a long strip of resistance sensor fabricated using the ionogel was installed on the knuckle of a hand to monitor finger movements. The relative resistance of the sensor was sensitive to the finger movements by angles of 15°, 30°, 60° and 90°. We also detected the electrical resistance signal of the recycled UiO-66-ionogel for finger bending. Notably, the sensing performance is almost unchanged between the original sensor and the recycled sensor, which validated the great potential of the UiO-66-ionogel sensor with recyclable properties in reducing electronic waste. Similar changes in sensitivity occurred when the sensor was attached to the wrist (Fig. 6i). These results imply that UiO-66-ionogels are a promising material for the fabrication of recyclable smart sensors.

Applicability of the coordination strategy

When UiO-66 was substituted by other MOFs, the mechanical properties of the ionogel were enhanced, as shown in Fig. S15 (ESI†). Upon the addition of UiO-66, the stress–strain characteristics of the ionogel were superior compared with those observed upon the addition of MIL-100(Fe) (Fe-MOF) and HKUST-1 (Cu-MOF). The differences in the stress–strain characteristics were attributed to the coordination of the polymer chains with the metal sites of the MOFs. To further illustrate the toughening effect of MOF on the ionogel, HKUST-1 is considered as an example. The stress and strain of the ionogel were tested when the contents of IL and HKUST-1 were changed, respectively (Fig. S16 and S17, ESI†). The obtained UiO-66-ionogel exhibited similar regularity. When the IL content was increased from 50 to 80 wt%, the strain increased from 520% to 985%, while the stress decreased from 3.5 MPa to 132 kPa. Meanwhile, the crosslinking density was influenced by the content of HKUST-1. The more the content of HKUST-1, the more the stress and the less the strain would be. Moreover, the ionogel exhibited excellent toughness and Young's modulus of 14.6 MJ m^{-3} and 46 MPa, respectively. As shown in Fig. S18 (ESI†), the tear resistance of the HKUST-1-ionogels with different IL contents was tested. The results indicated that HKUST-1 could also be used to effectively transfer applied stress uniformly to the surrounding segments while preventing severe stress concentration and reducing the formation of initial cracks. Therefore, the mechanical properties of the ionogels were significantly improved. As shown in Fig. S19 (ESI†), the good elasticity of the ionogels was maintained after 200% and 500% cyclic stretching. Here, we conclude that the MOF has the effect of toughening ionogels.

Conclusions

In this study, we prepared UiO-66 facilitated ionogels for recyclable sensors with excellent mechanical properties and tear resistance. The addition of UiO-66 introduced reversible interactions that prevent covalent crosslinking in the matrix polymer network. The coordination between UiO-66 and the polymer segments caused the formation of a new polymer network topology and enabled sufficient energy dissipation, and thus the ionogels are endowed with excellent mechanical properties. Moreover, the UiO-66 nanoparticles effectively prevented crack propagation during the tearing process. In addition, the polymer segments and UiO-66 can be recombined, which can enable the recovery and mechanical regeneration of waste ionogels. Therefore, UiO-66-ionogels have excellent mechanical properties, tear resistance, and recyclability and are excellent for application in flexible electronic devices.

Experimental section

Materials

N,*N*-Dimethylacrylamide (DMAA), 1-hydroxycyclohexyl phenyl ketone (HCPK), and 1-bromoacetonitrile were purchased from Energy Chemical. ZrCl$_4$, FeCl$_3$·6H$_2$O, 1-methylimidazole, and lithium bis(trifluoromethane sulfonimide) (LiTFSI) were purchased from Aladdin Chemistry Co., Ltd. Terephthalic acid (H$_2$BDC) was purchased from Sinopharm Chemical Reagent Co., Ltd. Trimesic acid (H$_3$BTC) was purchased from Meyer Chemical Technology Co., Ltd. Cu(NO$_3$)$_2$·3H$_2$O was purchased from Shanghai Macklin Biochemical Co., Ltd. The organic solvents (DMF, acetone, diethyl ether, ethanol) used in this work were obtained from commercial sources and used without further purification.

Characterizations

The mechanical properties of the prepared ionogels were tested on a tensile machine (Instron 5965) using a 50-N mechanical sensor. ^{1}H NMR spectra were performed at room temperature using DMSO-d$_6$ as a solvent on an AVANCE NEO 400 MHz nuclear magnetic resonance instrument. Powder X-ray diffraction (PXRD) data were obtained from 5° to 50° at a scanning speed of 5° min^{-1} using a Bruker D8 Advance diffractometer. Fourier transform infrared (FT-IR) spectra were performed on a Nicolet 5200 spectrometer in the range of 600–4000 cm^{-1}. Dynamic scanning calorimetry (DSC) curves of IL, DMAA, and ionogel between −60 and 20 °C were measured on DSC 4000 in a nitrogen atmosphere at a heating rate of 5 °C min^{-1}. Thermogravimetric analysis (TGA) was performed on PerkinElmer 4000 *via* heat from 30 to 800 °C at a heating rate of 10 °C min^{-1} under flowing N$_2$ and air, respectively. X-ray photoelectron spectroscopy (XPS) was performed using an XPS-7000 spectrometer with a Mg Kα X-ray source. Raman spectra were obtained using an Xplore plus Raman spectrometer with a 532 nm laser.

Synthesis of UiO-66 (Zr-MOF)

The synthesis of UiO-66 was according to the previously reported method.[62] Briefly, 30 mg ZrCl$_4$ and 20 mg H$_2$BDC were mixed in 10 mL DMF. Then, 1 mL acetic acid was added and sonicated for 10 min. All the mixture was transferred into a Teflon-lined autoclave. The Teflon-lined autoclave was sealed and heated in a vacuum at 120 °C for 12 h. The product was obtained by centrifugation after cooling down and washed with DMF and ethanol three times. Finally, UiO-66 was dried at 120 °C for 24 h under vacuum conditions. The product was confirmed by XRD (Fig. S2, ESI†).

Synthesis of MIL-100(Fe) (Fe-MOF)

The MIL-100 was synthesized according to the previously reported method.[63] Briefly, FeCl$_3$·6H$_2$O (4.04 g, 10 mmol), H$_3$BTC (1.89 g, 9 mmol), and deionized water (6 mL) were mixed by sonication for 10 min and moved into a 25 mL round bottom flask with a reflux condenser. The round bottom flask was reacted at 95 °C for 12 h. The product was obtained by centrifugation after cooling down and washed with deionized water and ethanol three times. Finally, MIL-100(Fe) was moved to a vacuum for 24 h at 150 °C. The product was confirmed by XRD (Fig. S2, ESI†).

Synthesis of HKUST-1 (Cu-MOF)

The HKUST-1 was synthesized according to the previously reported method with a little modification.[64] In a typical synthesis, $Cu(NO_3)_2 \cdot 3H_2O$ (2.174 g, 9 mmol) was mixed in 30 mL deionized water, and H_3BTC (1.05 g, 5 mmol) was mixed in 30 mL ethanol. The mixture was mixed together by sonication for 10 min. The product was obtained by centrifugation and washed with ethanol three times. Finally, the blue power was dried at 100 °C for 24 h under vacuum conditions. The product was confirmed by XRD (Fig. S2, ESI†).

Synthesis of 1-cyanomethyl-3-methylimidazolium bis[(trifluoromethyl)sulfonyl]imide ([CMMIM]TFSI)

1-Methylimidazole (10.43 g, 0.11 mol) and 1-bromoacetonitrile (12.00 g, 0.10 mol) were mixed in acetone solution (30 mL) and stirred at room temperature for 2 days. The solid product was washed with acetone and diethyl ether three times, then dried under a dynamic vacuum at 25 °C for 12 h to obtain a white solid powder.

[CMMIM]Br (18.18 g, 0.08 mol) was dissolved in deionized water, LiTFSI was added (25.84 g, 0.08 mol), and the mixture was stirred for 10 h at 25 °C for anion exchange. The mixture was washed three times with deionized water and dried under vacuum at 25 °C to get a transparent liquid 1-cyanomethyl-3-methylimidazoliumbis[(trifluoromethyl)sulfonyl]-imide ([CMMIM]TFSI). ^{1}H NMR (400 MHz, DMSO-d_6, δ):9.2 (s, 1H, N–CH=N), 7.9 (s, 1H, CH–CH=N), 7.7 (s, 1H, CH–CH=CH$_2$), 5.6 (m, 2H, N–CH$_2$–CN), 3.9 (t, 3H, CH$_2$–CH$_3$).

Synthesis of MOF-ionogel

The precursor solution was obtained by dissolving monomer DMAA, MOF, 1 wt% HCPK as initiator, and [CMMIM]TFSI as solvent. Next, the solution was reacted with a UV light source (365 nm) for 30 min to obtain the MOF-ionogel.

Molecular dynamics simulations

All MD simulations were conducted with the Materials Studio 2017 program. The interactions between solvents and MOFs were described by the COMPASS II force field, and the charge of all particles was given by the force field. Periodic boundary conditions in all three dimensions were implemented. The dimensions in the system were $41.08 \times 41.08 \times 160$ Å, which contains 239 DMAA, 136 [CMMIM]TFSI molecules, and $3 \times 3 \times 3$ MOFs. The temperature and pressure were controlled by A Nosé–Hoover thermostat and Berendsen barostat algorithm, respectively. The cutoff distance for pair interactions was set to 12.5 Å. The contribution of long-range interactions was calculated by tail correction and the particle–particle–particle–mesh (PPPM) solver. For each system, the system was equilibrated at 298 K in the *NVT* ensemble for 4 ns for equilibrium, and a subsequent 2 ns *NVT* simulation with external force (300 kcal mol^{-1} Å^{-1}) in a graphite plate was used to obtain the data.

Then, the interaction energy between the solvents and MOF was calculated according to the eqn (S1) (ESI†) at 25 °C and 101 kPa.

$$E_{inter} = E_{total} - (E_{solvent} + E_{MOF})$$

Among them, E_{inter} represents the interaction energy between the solvents and MOF. E_{total} is the total energy of the solvent-MOF system. $E_{solvent}$ is the energy of the solvent molecules. E_{MOF} is the energy of the MOFs.

Author contributions

Q. X., and W. L. contributed equally to this work. The manuscript was written through the contributions of all authors. All authors have given approval to the final version of the manuscript.

Conflicts of interest

There are no conflicts.

Acknowledgements

Notes and references

1 W. Qian, J. Texter and F. Yan, Frontiers in poly(ionic liquid)s: syntheses and applications, *Chem. Soc. Rev.*, 2017, **46**, 1124.

2 W. Qian, C. Yuan, J. Guo and F. Yan, A Review of Poly(Ionic Liquid)s Based Functional Materials, *Acta Chim. Sin.*, 2015, **73**, 310.

3 X. Yang, G. Liu, L. Peng, J. Guo, L. Tao, J. Yuan, C. Chang, Y. Wei and L. Zhang, Highly Efficient Self-Healable and Dual Responsive Cellulose-Based Hydrogels for Controlled Release and 3D Cell Culture, *Adv. Funct. Mater.*, 2017, **27**, 1703174.

4 J. Le Bideau, L. Viau and A. Vioux, Ionogels, ionic liquid based hybrid materials, *Chem. Soc. Rev.*, 2011, **40**, 907.

5 T. P. Lodge and T. Ueki, Mechanically Tunable, Readily Processable Ion Gels by Self-Assembly of Block Copolymers in Ionic Liquids, *Acc. Chem. Res.*, 2016, **19**, 2107.

6 B. Zhou, M. Yang, C. Zuo, G. Chen, D. He, X. Zhou, C. Liu, X. Xie and Z. Xue, Flexible, Self-Healing, and Fire-Resistant Polymer Electrolytes Fabricated via Photopolymerization for All-Solid-State Lithium Metal Batteries, *ACS Macro Lett.*, 2020, **9**, 525.

7 L. Shi, K. Jia, Y. Gao, H. Yang, Y. Ma, S. Lu, G. Gao, H. Bu, T. Lu and S. Ding, Highly Stretchable and Transparent Ionic Conductor with Novel Hydrophobicity and Extreme-Temperature Tolerance, *Research*, 2020, **2020**, 2505619.

8 M. Malischewski, M. Adelhardt, J. Sutter, K. Meyer and K. Seppelt, Isolation and structural and electronic

characterization of salts of the decamethylferrocene dication, *Science*, 2016, **353**, 678.

9 N. Chen, H. Zhang, L. Li, R. Chen and S. Guo, Ionogel Electrolytes for High-Performance Lithium Batteries: A Review, *Adv. Energy Mater.*, 2018, **8**, 1702675.

10 W. Li, L. Li, S. Zheng, Z. Liu, X. Zou, Z. Sun, J. Guo and F. Yan, Recyclable, Healable, and Tough Ionogels Insensitive to Crack Propagation, *Adv. Mater.*, 2022, **34**, e2203049.

11 L. M. Zhang, Y. He, S. Cheng, H. Sheng, K. Dai, W. J. Zheng, M. X. Wang, Z. S. Chen, Y. M. Chen and Z. Suo, Self-Healing, Adhesive, and Highly Stretchable Ionogel as a Strain Sensor for Extremely Large Deformation, *Small*, 2019, **15**, e1804651.

12 B. He, Y. Zhou, Z. Wang, Q. Wang, R. Shen and S. Wu, A multi-layered touch-pressure sensing ionogel material suitable for sensing integrated actuations of soft robots, *Sens. Actuators, A*, 2018, **272**, 341.

13 Z. Liu, Y. Wang, Y. Ren, G. Jin, C. Zhang, W. Chen and F. Yan, Poly(ionic liquid) hydrogel-based anti-freezing ionic skin for a soft robotic gripper, *Mater. Horiz.*, 2020, **7**, 919.

14 Y. M. Kim and H. C. Moon, Ionoskins: Nonvolatile, Highly Transparent, Ultrastretchable Ionic Sensory Platforms for Wearable Electronics, *Adv. Funct. Mater.*, 2019, **30**, 1907290.

15 Y. Zhao, C. Xuan, X. Qian, Y. Alsaid, M. Hua, L. Jin and X. He, Soft phototactic swimmer based on self-sustained hydrogel oscillator, *Sci. Robot.*, 2019, **4**, eaax7112.

16 M. Wang, P. Zhang, M. Shamsi, J. L. Thelen, W. Qian, V. K. Truong, J. Ma, J. Hu and M. D. Dickey, Tough and stretchable ionogels by in situ phase separation, *Nat. Mater.*, 2022, **21**, 359.

17 D. Weng, F. Xu, X. Li, S. Li, Y. Li and J. Sun, Polymeric Complex-Based Transparent and Healable Ionogels with High Mechanical Strength and Ionic Conductivity as Reliable Strain Sensors, *ACS Appl. Mater. Interfaces*, 2020, **12**, 57477.

18 H. Li, F. Xu, T. Guan, Y. Li and J. Sun, Mechanically and environmentally stable triboelectric nanogenerator based on high-strength and anti-compression self-healing ionogel, *Nano Energy*, 2021, **90**, 106645.

19 Y. Ding, J. Zhang, L. Chang, X. Zhang, H. Liu and L. Jiang, Preparation of High-Performance Ionogels with Excellent Transparency, Good Mechanical Strength, and High Conductivity, *Adv. Mater.*, 2017, **29**, 1704253.

20 Y. Sun, Y.-Y. Ren, Q. Li, R.-W. Shi, Y. Hu, J.-N. Guo, Z. Sun and F. Yan, Conductive, Stretchable, and Self-healing Ionic Gel Based on Dynamic Covalent Bonds and Electrostatic Interaction, *Chin. J. Polym. Sci.*, 2019, **37**, 1053.

21 L. Liu, Z. Liu, Y. Ren, X. Zou, W. Peng, W. Li, Y. Wu, S. Zheng, X. Wang, F. Yan and A. Superstrong, and Reversible Ionic Crystal-Based Adhesive Inspired by Ice Adhesion, *Angew. Chem., Int. Ed.*, 2021, **60**, 8948.

22 H. C. Yu, C. Y. Li, M. Du, Y. Song, Z. L. Wu and Q. Zheng, Improved Toughness and Stability of κ-Carrageenan/Poly-acrylamide Double-Network Hydrogels by Dual Cross-Linking of the First Network, *Macromolecules*, 2019, **52**, 629.

23 C. H. Yang, M. X. Wang, H. Haider, J. H. Yang, J. Y. Sun, Y. M. Chen, J. Zhou and Z. Suo, Strengthening alginate/polyacrylamide hydrogels using various multivalent cations, *ACS Appl. Mater. Interfaces*, 2013, **5**, 10418.

24 J. Y. Sun, X. Zhao, W. R. Illeperuma, O. Chaudhuri, K. H. Oh, D. J. Mooney, J. J. Vlassak and Z. Suo, Highly stretchable and tough hydrogels, *Nature*, 2012, **489**, 133.

25 H. C. Yu, S. Y. Zheng, L. Fang, Z. Ying, M. Du, J. Wang, K. F. Ren, Z. L. Wu and Q. Zheng, Reversibly Transforming a Highly Swollen Polyelectrolyte Hydrogel to an Extremely Tough One and its Application as a Tubular Grasper, *Adv. Mater.*, 2020, **32**, e2005171.

26 Y. Li, J. Yan, Y. Liu and X. M. Xie, Super Tough and Intelligent Multibond Network Physical Hydrogels Facilitated by Ti3C2Tx MXene Nanosheets, *ACS Nano*, 2021, **16**, 1567.

27 E. Kamio, T. Yasui, Y. Iida, J. P. Gong and H. Matsuyama, Inorganic/Organic Double-Network Gels Containing Ionic Liquids, *Adv. Mater.*, 2017, **29**, 1704118.

28 X. Jing, H.-Y. Mi, X.-F. Peng and L.-S. Turng, Biocompatible, self-healing, highly stretchable polyacrylic acid/reduced graphene oxide nanocomposite hydrogel sensors via mussel-inspired chemistry, *Carbon*, 2018, **136**, 63.

29 X. Liu, B. Wang, Z. Jin, H. Wang and Q. Wang, Elastic ionogels with freeze-aligned pores exhibit enhanced electrochemical performances as anisotropic electrolytes of all-solid-state supercapacitors, *J. Mater. Chem. A*, 2015, **3**, 15408.

30 H. Wang, J. Xu, K. Li, Y. Dong, Z. Du and S. Wang, Highly stretchable, self-healable, and self-adhesive ionogels with efficient antibacterial performances for a highly sensitive wearable strain sensor, *J. Mater. Chem. B*, 2022, **10**, 1301.

31 Y. Huang, M. Zhong, Y. Huang, M. Zhu, Z. Pei, Z. Wang, Q. Xue, X. Xie and C. Zhi, A self-healable and highly stretchable supercapacitor based on a dual crosslinked polyelectrolyte, *Nat. Commun.*, 2015, **6**, 10310.

32 M. Tavakoli, P. A. Lopes, A. Hajalilou, A. Silva, M. R. Carneiro, J. Carvalheiro, J. M. Pereira and A. T. de Almeida, 3R Electronics: Scalable Fabrication of Resilient, Repairable, and Recyclable Soft-Matter Electronics, *Adv. Mater.*, 2022, e2203266.

33 A. Terazono, S. Murakami, N. Abe, B. Inanc, Y. Moriguchi, S.-I. Sakai, M. Kojima, A. Yoshida, J. Li, J. Yang, M. H. Wong, A. Jain, I.-S. Kim, G. L. Peralta, C.-C. Lin, T. Mungcharoen and E. Williams, Current status and research on E-waste issues in, *Asia. J. Mater. Cycles. Waste*, 2006, **8**, 1–12.

34 B. H. Robinson, E-waste: An assessment of global production and environmental impacts, *Sci. Total Environ.*, 2009, **408**, 183.

35 A. Kumar, M. Holuszko and D. C. R. Espinosa, E-waste: An overview on generation, collection, legislation and recycling practices, *Resour., Conserv. Recycl.*, 2017, **122**, 32.

36 X. Zeng and J. Li, Measuring the recyclability of e-waste: an innovative method and its implications, *J. Clean. Prod.*, 2016, **131**, 156.

37 K. Zhang, J. L. Schnoor and E. Y. Zeng, E-waste recycling: where does it go from here?, *Environ. Sci. Technol.*, 2012, **46**, 10861.

38 Y. Hong, D. Thirion, S. Subramanian, M. Yoo, H. Choi, H. Y. Kim, J. F. Stoddart and C. T. Yavuz, Precious metal recovery from electronic waste by a porous porphyrin polymer, *Proc. Natl. Acad. Sci. U. S. A.*, 2020, **117**, 16174.

39 X. Aeby, A. Poulin, G. Siqueira, M. K. Hausmann and G. Nystrom, Fully 3D Printed and Disposable Paper Supercapacitors, *Adv. Mater.*, 2021, **33**, e2101328.

40 M.-M. Xu, Q. Chen, L.-H. Xie and J.-R. Li, Exchange reactions in metal–organic frameworks: New advances. Coordin, *Chem. Rev.*, 2020, **421**, 213421.

41 Z. Wang, Y. Wu, K. Xu, L. Jiang, J. Sun, G. Cai, G. Li, B. Y. Xia and H. Liu, Hierarchical Oriented Metal–Organic Frameworks Assemblies for Water-Evaporation Induced Electricity Generation, *Adv. Funct. Mater.*, 2021, **31**, 2104732.

42 Q. Ma, Q. He, P. Yin, H. Cheng, X. Cui, Q. Yun and H. Zhang, Rational Design of MOF-Based Hybrid Nanomaterials for Directly Harvesting Electric Energy from Water Evaporation, *Adv. Mater.*, 2020, **32**, e2003720.

43 J. A. Neal, N. J. Oldenhuis, A. L. Novitsky, E. M. Samson, W. J. Thrift, R. Ragan and Z. Guan, Large Continuous Mechanical Gradient Formation via Metal-Ligand Interactions, *Angew. Chem., Int. Ed.*, 2017, **56**, 15575.

44 J.-K. Sun, H.-J. Lin, W.-Y. Zhang, M.-R. Gao, M. Antonietti and J. Yuan, A tale of two membranes: from poly (ionic liquid) to metal–organic framework hybrid nanoporous membranesviapseudomorphic replacement, *Mater. Horiz.*, 2017, **4**, 681.

45 Y. Cao, H. Wu, G. Li, C. Liu, L. Cao, Y. Zhang, W. Bao, H. Wang, Y. Yao, S. Liu, F. Pan, Z. Jiang and J. Sun, Ion Selective Covalent Organic Framework Enabling Enhanced Electrochemical Performance of Lithium-Sulfur Batteries, *Nano Lett.*, 2021, **21**, 2997.

46 Y. Guo, X. Zou, W. Li, Y. Hu, Z. Jin, Z. Sun, S. Gong, S. Guo and F. Yan, High-density sulfonic acid-grafted covalent organic frameworks with efficient anhydrous proton conduction, *J. Mater. Chem. A*, 2022, **10**, 6499.

47 L. Xu, Z. Huang, Z. Deng, Z. Du, T. L. Sun, Z. H. Guo, K. Yue and A. Transparent, Highly Stretchable, Solvent-Resistant, Recyclable Multifunctional Ionogel with Underwater Self-Healing and Adhesion for Reliable Strain Sensors, *Adv. Mater.*, 2021, **33**, e2105306.

48 B. Yiming, X. Guo, N. Ali, N. Zhang, X. Zhang, Z. Han, Y. Lu, Z. Wu, X. Fan, Z. Jia and S. Qu, Ambiently and Mechanically Stable Ionogels for Soft Ionotronics, *Adv. Funct. Mater.*, 2021, **31**, 2102773.

49 B. Yiming, Y. Han, Z. Han, X. Zhang, Y. Li, W. Lian, M. Zhang, J. Yin, T. Sun, Z. Wu, T. Li, J. Fu, Z. Jia and S. Qu, A Mechanically Robust and Versatile Liquid-Free Ionic Conductive Elastomer, *Adv. Mater.*, 2021, **33**, e2006111.

50 K. G. Cho, S. An, D. H. Cho, J. H. Kim, J. Nam, M. Kim and K. H. Lee, Block Copolymer-Based Supramolecular Ionogels for Accurate On-Skin Motion Monitoring, *Adv. Funct. Mater.*, 2021, **31**, 2106382.

51 M. Zhang, X. Tao, R. Yu, Y. He, X. Li, X. Chen and W. Huang, Self-healing, mechanically robust, 3D printable ionogel for highly sensitive and long-term reliable ionotronics, *J. Mater. Chem. A*, 2022, **10**, 12005.

52 M. Li, L. Chen, Y. Li, X. Dai, Z. Jin, Y. Zhang, W. Feng, L. T. Yan, Y. Cao and C. Wang, Superstretchable, yet stiff,

fatigue-resistant ligament-like elastomers, *Nat. Commun.*, 2022, **13**, 2279.

53 S. Y. Zheng, S. Mao, J. Yuan, S. Wang, X. He, X. Zhang, C. Du, D. Zhang, Z. L. Wu and J. Yang, Molecularly Engineered Zwitterionic Hydrogels with High Toughness and Self-Healing Capacity for Soft Electronics Applications, *Chem. Mater.*, 2021, **33**, 8418.

54 K. Sato, T. Nakajima, T. Hisamatsu, T. Nonoyama, T. Kurokawa and J. P. Gong, Phase-Separation-Induced Anomalous Stiffening, Toughening, and Self-Healing of Polyacrylamide Gels, *Adv. Mater.*, 2015, **27**, 6990.

55 J. Kang, D. Son, G. N. Wang, Y. Liu, J. Lopez, Y. Kim, J. Y. Oh, T. Katsumata, J. Mun, Y. Lee, L. Jin, J. B. Tok and Z. Bao, Tough and Water-Insensitive Self-Healing Elastomer for Robust Electronic Skin, *Adv. Mater.*, 2018, **30**, e1706846.

56 M. Li, J. Li, H. Na and J. J. Vlassak, Mechanical behavior of poly(methyl methacrylate)-based ionogels, *Soft Matter*, 2014, **10**, 7993.

57 Z. Cao, H. Liu and L. Jiang, Transparent, mechanically robust, and ultrastable ionogels enabled by hydrogen bonding between elastomers and ionic liquids, *Mater. Horiz.*, 2020, **7**, 912.

58 S. Lin, C. Cao, Q. Wang, M. Gonzalez, J. E. Dolbow and X. Zhao, Design of stiff, tough and stretchy hydrogel composites *via* nanoscale hybrid crosslinking and macroscale fiber reinforcement, *Soft Matter*, 2014, **10**, 7519.

59 A. Klein, P. G. Whitten, K. Resch and G. Pinter, Nanocomposite hydrogels: Fracture toughness and energy dissipation mechanisms, *J. Polym. Sci., B: Polym. Phys.*, 2015, **53**, 1763.

60 Y. Zhang, Y. Li and W. Liu, Dipole-Dipole and H-Bonding Interactions Significantly Enhance the Multifaceted Mechanical Properties of Thermoresponsive Shape Memory Hydrogels, *Adv. Funct. Mater.*, 2015, **25**, 471.

61 N. Annabi, S. R. Shin, A. Tamayol, M. Miscuglio, M. A. Bakooshli, A. Assmann, P. Mostafalu, J. Y. Sun, S. Mithieux, L. Cheung, X. S. Tang, A. S. Weiss and A. Khademhosseini, Highly Elastic and Conductive Human-Based Protein Hybrid Hydrogels, *Adv. Mater.*, 2016, **28**, 40.

62 X. Peng, L. Ye, Y. Ding, L. Yi, C. Zhang and Z. Wen, Nanohybrid photocatalysts with ZnIn2S4 nanosheets encapsulated UiO-66 octahedral nanoparticles for visible-light-driven hydrogen generation, *Appl. Catal., B*, 2020, **260**, 118152.

63 C. Yue, L. Wu, Y. Lin, Y. Lu, C. Shang, R. Ma, X. Zhang, X. Wang, W. D. Wu, X. D. Chen and Z. Wu, Study on the Stability, Evolution of Physicochemical Properties, and Post-synthesis of Metal–Organic Frameworks in Bubbled Aqueous Ozone Solution, *ACS Appl. Mater. Interfaces*, 2021, **13**, 26264.

64 M. Bagheri, A. Melillo, B. Ferrer, M. Y. Masoomi and H. Garcia, Improved catalytic hydrogen release of quasi HKUST-1 compared to HKUST-1, *Chem. Commun.*, 2021, **57**, 11964.